Prediction of structure candidates for zinc oxide as a function of pressure and investigation of their electronic properties

D. Zagorac,* J. C. Schön, J. Zagorac, and M. Jansen
Max Planck Institute for Solid State Research, Stuttgart, Germany
(Received 29 August 2013; revised manuscript received 13 January 2014; published 3 February 2014)

In order to gain new insight in the ZnO system, we performed crystal structure prediction using simulated annealing with an empirical potential and local optimization on *ab initio* level, both at standard and elevated pressure. We have found the experimentally observed structure types [wurtzite (B4), sphalerite (B3), and rock salt (B1)] in agreement with previous research. In addition, many new interesting modifications were found in different regions of the energy landscape, such as the β-BeO type, the GeP type, the NiAs type, and the so-called "5-5" type modification. At extreme conditions (>150 GPa), we observe a CsCl (B2) type of structure, and as a possible intermediate phase along the NaCl (B1) $\rightarrow$ CsCl (B2) transition route, we suggest the α-WC (B_h) modification. Furthermore, we have investigated the electronic properties of ZnO structures. Our investigations offer new possibilities of tuning the band gap with pure zinc oxide by employing modifications with different structural arrangements.

DOI: 10.1103/PhysRevB.89.075201 PACS number(s): 61.50.Ah, 61.66.Fn, 61.50.Ks, 71.15.Nc

I. INTRODUCTION

Zinc oxide (ZnO) is a wide band gap semiconductor (E_{gap} = 3.3 eV at room temperature) with a large number of desirable properties for industrial applications (e.g., transparency, luminescence, high electron mobility, etc.). Therefore, it is successfully employed in electronics [e.g., light-emitting diodes, liquid crystal displays, etc.], batteries, and optical systems. In addition, ZnO powder is commonly used as an additive to various materials such as rubber, ceramics, paints, glasses, cements, creams, pigments, food, etc. [1–5]. As a consequence, zinc oxide is one of the most studied systems, both experimentally [6–15] and theoretically [16–26].

In nature, zinc oxide appears as the mineral zincite, which exhibits a hexagonal crystal structure and whose color depends on the presence of impurities such as MnO, FeO, and SiO_2. Since their amount is usually less than 1%, zincite is translucent, transparent in thin fragments, with a color ranging from yellow-orange to red and, extremely rarely found, yellow, green, or colorless [27–29]. The ideal bulk zinc oxide, without impurities, adopts the hexagonal wurtzite type of structure at ambient conditions [see Fig. 1(a)] [30,31].

In the experiments performed thus far, a well-known phase transition is observed from the wurtzite-type (B4) to the rock salt-type (B1) modification at a pressure of about 10 GPa [see Fig. 1(b)] [1,32–35]. In addition, a sphalerite-type modification (B3) can be stabilized by growing ZnO on substrates with cubic lattice structure, resulting in nanocrystalline ZnO thin films [see Fig. 1(c)] [36–39]. Furthermore, very thin films (<15 atomic layers) of a ZnO modification exhibiting the 5-5 structure type [the ionic analogue to the hexagonal boron nitride (*h*-BN) structure [40,41]] have been recently synthesized [42–44].

From the theoretical point of view, the focus has been on the properties of the wurtzite modification, the simulation of the growth of ZnO films, the investigation of the B4–B1 transition, and on structures and properties of $(ZnO)_n$ clusters [16–26]. Furthermore, a transition to a CsCl type (B2) of structure and some other high pressure ZnO modifications have been proposed to occur at very high pressures (>200 GPa) [19,45–51], which has been followed by some experimental observations at very high pressures [52]. Nevertheless, there are a number of open questions regarding, e.g., the possibility of intermediary structures along the B4–B1 transition route and the existence of the 5-5-type modification as a bulk phase. Quite generally, the existence of alternative (meta)stable modifications of zinc oxide and their properties is still an open issue. Furthermore, in particular the electronic properties of such modifications might be useful for technological applications of zinc oxide.

In preliminary work we had proposed a number of interesting new structure candidates for ZnO, such as the β-beryllium oxide (BeO) type, the nickel arsenide (NiAs) type, and the so-called 5-5 type, as well as several polytypes corresponding to alternative stackings of the known wurtzite and sphalerite modifications [53,54]. In the current study, we perform large scale global explorations of the energy landscape of ZnO and determine in this way possible (meta)stable modifications of ZnO for the full pressure range from effective negative pressures to high positive pressures. Besides the thermodynamic stability, we analyze structural and electronic properties of these new modifications.

II. THEORETICAL METHODS

Quite generally, all stable and metastable modifications of a chemical system correspond to the locally ergodic regions on the energy/enthalpy landscape of the system [55,56]. In particular, local minima surrounded by sufficiently high energy barriers represent possible structures that are (meta)stable at low or medium temperatures. Thus, our general approach to the determination of structure candidates is based on the search for local minima and proceeds via the global exploration of the energy landscape of the system of interest. The method has been given in detail elsewhere [55,56]; here, we provide

*Corresponding author: dejan.zagorac@fau.de

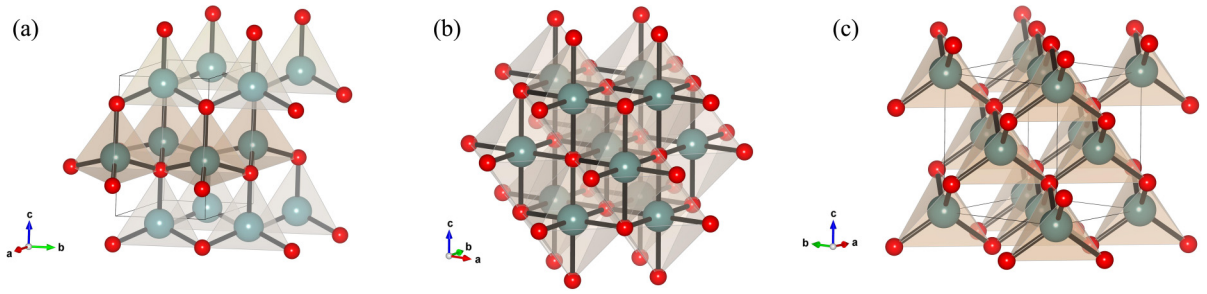

FIG. 1. (Color online) Visualization of the experimentally observed structure types in the ZnO system: (a) wurtzite type; (b) rock salt type; (c) sphalerite type. Note that the structures are represented in the periodically repeated cell.

information specific to this study. The minima were identified using simulated annealing (SA) as a global optimization procedure [57,58].

Since the global search involved many millions of energy evaluations, we employed an empirical energy/enthalpy function, $E = E_{\text{pot}} + pV$, in this study. Here, $E_{\text{pot}} = \Sigma_{\langle i,j \rangle} V_{ij}(r_{ij})$, where V_{ij} is a two-body empirical potential consisting of Lennard-Jones and Coulomb terms, and where, for the evaluation of the Coulomb summation, the method proposed by de Leeuw was employed [59]:

$$V_{ij}(r_{ij}) = \frac{q_i q_j}{4\pi\varepsilon_0 r_{ij}} + \varepsilon \cdot \left[\left(\frac{\sigma_{ij}}{r_{ij}} \right)^{12} - \left(\frac{\sigma_{ij}}{r_{ij}} \right)^{6} \right].$$

Here, q_i and q_j are the charges of the ions, r_{ij} is the distance between atoms i and j, $\sigma_{ij} = r_s(i) \cdot r_{\text{ion}}(i) + r_s(j) \cdot r_{\text{ion}}(j)$ is the scaled sum of the ionic radii, and ε gives the strength of the Lennard-Jones potential (see Tables V and VI of the Appendix for the values of the parameters) [40]. The reason for the introduction of the radius scale factor is the observation that the "ionic radii" found in tables can depend on the type of compound in which the atom participates. Therefore, if one studies the energy landscape globally of an (in principle) unknown chemical system using generic empirical potentials, one needs to repeat these searches for different values of the ionic radius parameters employed in the potential [40,60]. Regarding the number of atoms in the simulation cell, we performed the global optimizations for 1, 2, 3, 4, and 5 formula units ZnO per simulation cell.

Besides the calculations at standard pressure, the global optimizations were performed for a wide range of pressures (−10 GPa, +1 MPa, +10 MPa, +100 MPa, +1 GPa, +10 GPa, +100 GPa, +1000 GPa). Both the atom positions [70% of all Monte Carlo (MC) steps move an individual atom; 10% swap the positions of two atoms] and the parameters of the periodically repeated simulation cell (20% of all MC steps) were freely varied during the random walks. Each simulated annealing run consisted of 4×10^6 MC steps followed by 10 000 stochastic quench steps. For the global optimization, we have used the modular G-42 code [55].

Subsequent to the global search, the candidates found were locally optimized on *ab initio* level, and the $E(V)$ and $H(p)$ curves for the various modifications were computed to be able to determine the thermodynamically stable ones as function of pressure. For this, we employed the program CRYSTAL09 [61,62], which is based on linear combinations of atomic orbitals, and for the local optimizations we employed analytical gradients [63–66]. Each local optimization is performed on the Hartree-Fock (HF) and the density functional theory (DFT) level using the local density approximation (LDA). Here we used the Slater local exchange approximation [67,68] and Perdew-Zunger correlation functionals [69]. In addition, we have employed a hybrid B3LYP functional (Becke's three-parameter functional in combination with the correlation functional of Lee, Yang, and Parr [70]). It is reasonable to use several different *ab initio* methods to get some feeling for the quantitative validity of the results [71,72].

For these local optimizations, an all-electron basis set based on Gaussian-type orbitals was employed. In the case of Zn^{2+}, a $[6s5p2d]$ basis set was used, as in Refs. [73] and [74], and for O^{2-} a $[4s3p]$ basis set was used, as in Refs. [75] and [76], respectively (see also Supplemental Material [77]). During local optimizations, an $8 \times 8 \times 8$ k-point sampling net was used. In addition, a smearing temperature of 0.01 E_h was applied during the local optimization and the calculation of the $E(V)$ and $H(p)$ curves to facilitate the numerical integration. We note that the changes of initial computational parameters (k-point sampling net, smearing temperature, etc.), effect stability of calculated structures, and that the chosen $8 \times 8 \times 8$ k-point sampling net shows the best agreement with known experimental and theoretical results.

Both after the global optimizations and after the local minimizations, the symmetries and the space group of the structures found were determined using the algorithms SFND and RGS [78], respectively; duplicate structures were removed using the CMPZ algorithm [79]. All three algorithms are implemented in the program KPLOT [80]. Since there are usually a very large number of structural candidates, the symmetry analysis and part of the local optimizations were automatically performed with a heuristic algorithm (LOAD and FILTER programs) [71]. For the analysis of the structures and their visualization, we used the KPLOT [80] and VESTA [81] programs.

III. ANALYSIS OF POLYMORPHS AND PHASE TRANSITIONS

A. Results

Global searches were performed at seven different pressure (p) settings (from −10 GPa till 1000 GPa), with five different settings for radius scale factor (r_s) and five different sizes of unit cell (Z), where for each set of p, r_s, and Z, 400 SA runs were employed. In this section, the focus is on the polymorphs

TABLE I. Structure data of the energetically most favorable modifications of zinc oxide found after local optimizations performed using Hartree-Fock (HF), DFT (LDA), and hybrid (B3LYP) functional.

Space group, formula unit	Cell parameters, Wyckoff positions, and fractional coordinates		
(Z), and prototype	LDA	B3LYP	HF
$P6_3mc$ (186)	$a = 3.19$ Å, $c = 5.18$ Å	$a = 3.28$ Å, $c = 5.29$ Å	$a = 3.29$ Å, $c = 5.24$ Å
$Z = 2$	Zn (2*b*) 1/3, 2/3, 0	Zn (2*b*) 1/3, 2/3, 0	Zn (2*b*) 1/3, 2/3, 0
Wurtzite	O (2*b*) 1/3, 2/3, 0.3763	O (2*b*) 1/3, 2/3, 0.3787	O (2*b*) 1/3, 2/3, 0.3843
F-43m (216)	$a = 4.49$ Å	$a = 4.61$ Å	$a = 4.62$ Å
$Z = 4$	Zn (4*a*) 0, 0, 0	Zn (4*a*) 0, 0, 0	Zn (4*a*) 0, 0, 0
Sphalerite	O (4*c*) 3/4, 3/4, 3/4	O (4*c*) 3/4, 3/4, 3/4	O (4*c*) 3/4, 3/4, 3/4
Fm-3m (225)	$a = 4.23$ Å	$a = 4.33$ Å	$a = 4.30$ Å
$Z = 4$	Zn (4*b*) 1/2, 1/2, 1/2	Zn (4*b*) 1/2, 1/2, 1/2	Zn (4*b*) 1/2, 1/2, 1/2
NaCl	O (4*a*) 0, 0, 0	O (4*a*) 0, 0, 0	O (4*a*) 0, 0, 0
$I4mm$ (107)	$a = 2.85$ Å, $c = 4.98$ Å	$a = 2.92$ Å, $c = 5.10$ Å	$a = 2.92$ Å, $c = 4.91$ Å
$Z = 2$	Zn (2*a*) 0, 0, 0	Zn (2*a*) 0, 0, 0	Zn (2*a*) 0, 0, 0
GeP	O (2*a*) 0, 0, 0.3969	O(2*a*) 0, 0, 0.4002	O(2*a*) 0, 0, 0.4185
$P6_3/mmc$ (194)	$a = 3.40$ Å, $c = 4.39$ Å	$a = 3.48$ Å, $c = 4.54$ Å	$a = 3.48$ Å, $c = 4.46$ Å
$Z = 2$	Zn (2*d*) 1/3, 2/3, 3/4	Zn (2*d*) 1/3, 2/3, 3/4	Zn (2*d*) 1/3, 2/3, 3/4
5-5	O (2*c*) 2/3, 1/3, 3/4	O (2*c*) 2/3, 1/3, 3/4	O (2*c*) 2/3, 1/3, 3/4
$P6_3/mmc$ (194)	$a = 2.94$ Å, $c = 5.07$ Å	$a = 3.02$ Å, $c = 5.20$ Å	$a = 2.99$ Å, $c = 5.20$ Å
$Z = 2$	Zn (2*a*) 0, 0, 0	Zn (2*a*) 0, 0, 0	Zn (2*a*) 0, 0, 0
NiAs	O (2*c*) 1/3, 2/3, 1/4	O (2*c*) 1/3, 2/3, 1/4	O (2*c*) 1/3, 2/3, 1/4
$P4_2/mmm$ (136)	$a = 5.45$ Å, $c = 3.20$ Å	$a = 5.61$ Å, $c = 3.28$ Å	$a = 5.60$ Å, $c = 3.29$ Å
$Z = 4$	Zn (4*f*) 0.6813, 0.3187, 0	Zn (4*f*) 0.8194, 0.8194, 0	Zn (4*f*) 0.8201, 0.1799, 0
BeO	O (4*f*) 0.6825, 0.6825, 0	O (4*f*) 0.3164, 0.3164, 1/2	O (4*f*) 0.8168, 0.8168, 0
Pm-3m (221)	$a = 2.61$ Å	$a = 2.68$ Å	$a = 2.66$ Å
$Z = 1$	Zn (1*a*) 0, 0, 0	Zn (1*a*) 0, 0, 0	Zn (1*a*) 0, 0, 0
CsCl	O (1*b*) 1/2, 1/2, 1/2	O (1*b*) 1/2, 1/2, 1/2	O (1*b*) 1/2, 1/2, 1/2

generated and the possible phase transitions among them. The complete statistical analysis of the optimization process, together with calculated total energies and bulk moduli, is presented in the Appendix.

1. Modifications found at standard and elevated pressures

Table I presents the structural data for the most important modifications observed during the simulated annealing runs. Their corresponding energies calculated with HF, DFT (LDA), and the hybrid (B3LYP) functional are summarized in Table VII of the Appendix, while their corresponding volumes, temperatures, and bulk moduli are shown in Table VIII of the Appendix. Additional structures that represent new structure types but are higher in energy are shown in Table II. Figure 2 depicts the $E(V)$ and the $H(p)$ curves for the most important modifications at the B3LYP level; the corresponding results using HF and the LDA functional are given in the Supplemental Material [77].

Our calculations show that the experimentally observed bulk polymorphs of zinc oxide are the energetically lowest and thermodynamically most stable ones, which is in agreement with experiments [1,27–44] and previous calculations [16–26,45–52]. In particular, the wurtzite type with the sphalerite type are the stable modifications at ambient conditions (see Figs. 1 and 2).

Experimentally, the rock salt modification is observed as the most stable form at pressures above 10 GPa [1,32–35]. For the calculations performed using the HF approximation, we observe a transition from the wurtzite type to the rock salt type at about 9 GPa and with the B3LYP functional at about 12.5 GPa, respectively (see Fig. 2). When using the LDA functional, this transition takes place at about 9.5 GPa (see the Supplemental Material [77]). All of these results are in good agreement with experimental observations and previous calculations.

However, in the calculations performed with the LDA functional, we observe an earlier transition from the wurtzite- to the germanium phosphide (GeP)-type modification at about 8.5 GPa and then later a transition from the GeP to the NaCl structure type at about 12 GPa (see Supplemental Material [77]). The germanium phosphide (GeP) structure type can be described as a distorted variant of the rock salt (NaCl) type, which exhibits a $5+1$ coordination of Zn atoms by O atoms (ZnO_4 square pyramids) and crystallizes in space group $I4mm$ (no. 107) [see Fig. 3(a)]. This modification has also been observed in recent theoretical studies [18,25,82–86]; however, it has not been identified as the GeP structure type, but rather as an unknown tetragonal phase, which can cause misunderstandings, since another completely different tetragonal phase also appears on the energy landscape of zinc oxide in the form of the β-BeO structure type (see below) [87].

In addition, we have found several new hypothetical modifications in the ZnO system at elevated pressures. One of them is the NiAs (B_{81}) structure type that appeared as a metastable modification at standard conditions [see Fig. 3(b)] and also at extremely high pressures. According to our calculations, this modification is metastable even with an

TABLE II. Additional structure candidates of zinc oxide found at extreme conditions. Local optimizations were performed with Hartree-Fock (HF), DFT (LDA), and hybrid (B3LYP) functional.

Space group, formula unit	Cell parameters, Wyckoff positions and fractional coordinates		
(Z), and prototype	LDA	B3LYP	HF
P-6*m*2 (187)	$a = 2.89$ Å, $c = 2.64$ Å	$a = 2.97$ Å, $c = 2.69$ Å	$a = 2.95$ Å, $c = 2.69$ Å
$Z = 1$	Zn (1*a*) 0, 0, 0	Zn (1*a*) 0, 0, 0	Zn (1*a*) 0, 0, 0
α-WC	O (1*d*) 1/3, 2/3, 1/2	O (1*d*) 1/3, 2/3, 1/2	O (1*d*) 1/3, 2/3, 1/2
*R*3*m* (160)	[a]	$a = 3.07$ Å, $\alpha = 59.96°$	[a]
$Z = 1$		Zn (1*a*) 0, 0, 0	
α-GeTe		O (1*a*) 0.4833, 0.4833, 0.4833	
$P2_1/m$ (11)	$a = 2.99$ Å, $b = 3.84$ Å,	[a]	[a]
$Z = 2$	$c = 2.96$ Å, $\beta = 92{,}40°$		
ZnO-I	Zn (2*e*) 0.7057, ¾, 0.8055		
	O (2*e*) 0.2346, ¾, 0.2425		
$C2/m$ (12)	[a]	$a = 4.36$ Å, $b = 4.16$ Å,	[a]
$Z = 2$		$c = 3.22$ Å, $\beta = 132.41°$	
ZnO-II		Zn (2*a*) 0, 0, 0	
		O (2*b*) 1/2, 0, 0	
Pnma (62)	$a = 5.51$ Å, $b = 2.84$ Å,	$a = 5.76$ Å, $b = 3.02$ Å,	$a = 5.76$ Å, $b = 2.92$ Å,
$Z = 4$	$c = 5.54$ Å	$c = 5.23$ Å	$c = 5.29$ Å
ZnO-III	Zn (4*c*) 0.6508, ¾, 0.6735	Zn (4*c*) 0.6597, ¾, 0.6783	Zn (4*c*) 0.6362, ¾, 0.6927
	O (4*c*) 0.6339, ¾, 0.3149	O (4*c*) 0.6067, ¾, 0.2833	O (4*c*) 0.6327, ¾, 0.3001
*Imm*2 (44)	$a = 8.97$ Å, $b = 3.08$ Å,	$a = 9.14$ Å, $b = 3.26$ Å,	$a = 9.21$ Å, $b = 3.29$ Å,
$Z = 4$	$c = 5.38$ Å	$c = 5.45$ Å	$c = 5.38$ Å
ZnO-IV	Zn1 (4*c*) 0.6909, 0, 0	Zn1 (4*c*) 0.6920, 0, 0	Zn1 (4*c*) 0.6923, 0, 0
	Zn2 (2*b*) 1/2, 0, 0.4909	Zn2 (2*b*) 0, 1/2, 0.9871	Zn2 (2*b*) 1/2, 0, 0.4855
	O1 (4*c*) 0.3083, 0, 0.6378	O1 (4*c*) 0.3075, 0, 0.6302	O1 (4*c*) 0.3076, 0, 0.6242
	O2 (2*b*) 0, 1/2, 0.6468	O2 (2*b*) 0, 1/2, 0.6422	O2 (2*b*) 0, 1/2, 0.6376

[a]When the structure was optimized on this specific level of theory, it changed to the NaCl structure type.

increase of temperature and/or pressure; therefore, it would be very hard to synthesize, although the sixfold coordination of the zinc atoms by the oxygen atoms suggests that it might be present at high pressures in the ZnO system.

Another interesting modification found during global optimizations at high pressures (10 GPa; as well as in the prescribed path investigations of ZnO [87]) exhibits a slightly distorted version of the α-GeTe structure type [see Fig. 3(c)]. However, at standard pressure, this modification was a stable minimum only for the hybrid (B3LYP) functional. So far, there exist no experimental or calculated data regarding this type of structure in the ZnO or the related ZnS system. The ideal α-GeTe structure (*hR*6) can be described as a rhombohedrally sheared rock salt structure, with 3+3-fold coordination of

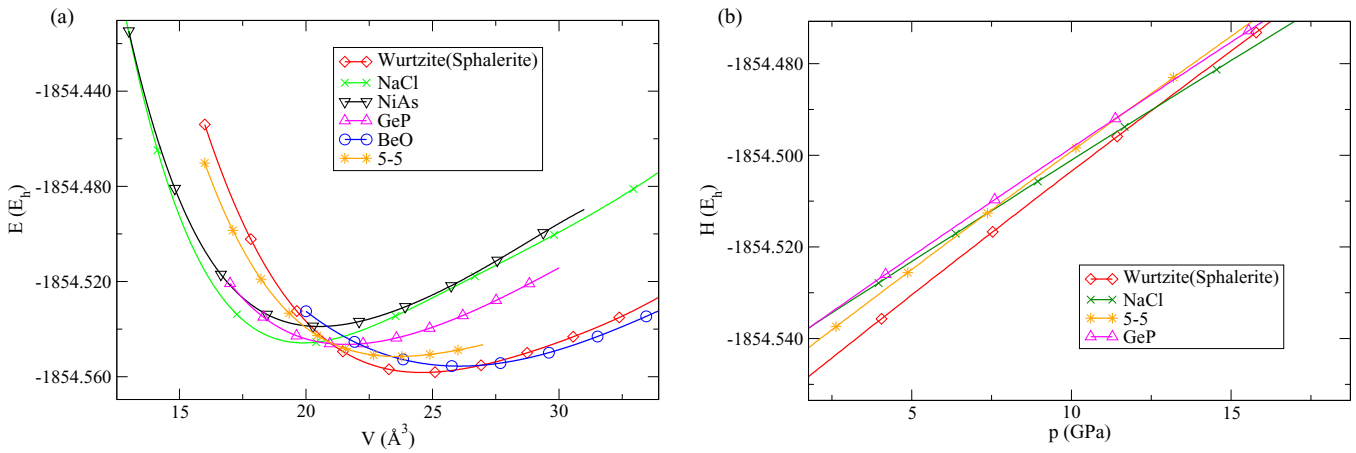

FIG. 2. (Color online) (a) $E(V)$ and (b) $H(p)$ curves at B3LYP level for the most relevant structure types at high pressures. Energies per formula unit are given in hartrees (E_h). Note that wurtzite and sphalerite modification exhibit essentially the same $E(V)$ curves at this level of calculation and are indistinguishable on the scale of the figure and therefore only the curve for wurtzite has been plotted.

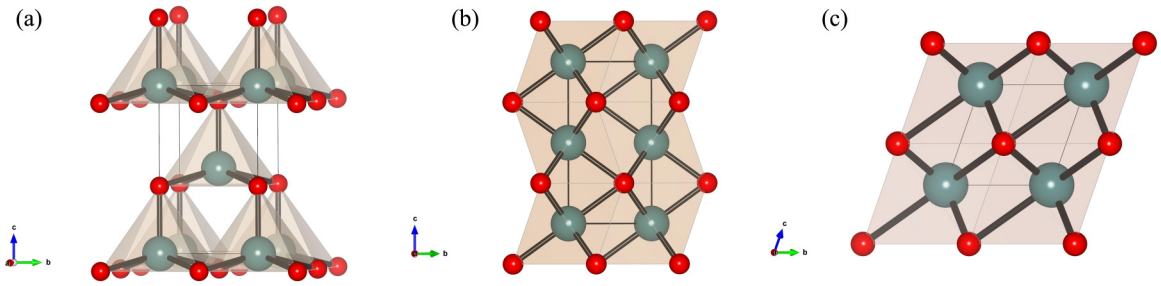

FIG. 3. (Color online) Visualization of alternative structure types found at high pressures: (a) GeP type; (b) NiAs type; (c) α-GeTe type.

the cations by the anions in the $R3m$ space group [88]. In the case of zinc oxide, this structure is slightly squeezed, resulting in a 3+3(+1) coordination of the zinc atoms by the oxygen atoms due to the high pressures applied. This cubic-to-rhombohedral phase transition is found experimentally in other AB compounds, e.g., germanium telluride [89,90], and has been theoretically predicted for lead sulfide [91,92].

2. *Calculated ZnO modifications at extreme conditions*

At extreme conditions (pressures of 100 GPa and 1000 GPa), the global optimizations yielded structure candidates where the zinc atoms were coordinated by six, seven, or eight oxygen atoms. The most relevant ones were of the CsCl type, the ZnO-I type, the ZnO-II type, and the ZnO-III type (see Fig. 4 and Tables I and II) plus several distorted configurations, some of which could be visually related to known structure candidates found in other AB compounds during earlier studies at elevated pressures [41,91,93]. Thus, we have optimized several of these structural candidates in the ZnO system; among these, the α-WC type was the lowest with respect to energy in zinc oxide. On *ab initio* level (using the LDA functional), the CsCl-type modification has been suggested to be thermodynamically stable at pressures beyond 200 GPa [19,45–51], which is in agreement with our DFT calculations. Employing the B3LYP functional leads to a NaCl $\rightarrow$ CsCl transition at about 150 GPa; however, when using the HF approximation, one encounters convergence problems at very small volumes for the CsCl structure, making it infeasible to assign a well-defined transition pressure at the HF level.

We note that the ZnO-I-type and ZnO-II-type structures appear to be distortions of the rock salt phase at extreme pressures. Both of the structures exhibit a monoclinic lattice, where ZnO-I has space group $P2_1/m$ (no. 11) and ZnO-II has space group $C2/m$ (no. 12), respectively. The ZnO-I modification was more stable than the rock salt structure for the LDA and HF approximation and relaxed to the rock salt modification when using the hybrid functional (see Table II). Similarly, the ZnO-II modification was stable for the B3LYP functional and converted to the NaCl modification otherwise. This suggests that both candidates are unlikely to be observed experimentally as a quenched phase outside the high pressure range.

As a more likely high pressure candidate at extreme conditions (>100 GPa), we suggest the α-WC-type modification (see Fig. 4 and Table II). The α-WC type (B_h) is a low temperature polymorph of tungsten carbide [94], which in ZnO should appear along the NaCl $\rightarrow$ CsCl transition route. Furthermore, the ZnO-III type of structure is likely to exist as a metastable phase in ZnO at pressures above 10 GPa. This unknown structure type has a fivefold coordination of Zn^{2+} by O^{2-} and, conversely, can be described with corner- and edge-sharing square pyramids; very similar arrangements of square pyramids have been observed on the enthalpy landscapes of NaCl [40]. We note that the ZnO-III type was obtained after relaxation of a FeB type of structure (see Table II).

3. *Modifications observed at effective negative pressures*

At effective negative pressures, we find several new candidates for stable modifications in the ZnO system during the global optimization. Among these, the most important ones exhibit the β-BeO, the 5-5, and the ZnO-IV structure type [see Figs. 4(c), 5(a), and 5(b)]. The β-BeO type exhibits space group $P4_2/mnm$ and, like the wurtzite type, is based on a hexagonal close packing of the oxygen anions. The Zn cations are located in neighboring tetrahedral interstices of this packing, resulting in pairs of edge-connected ZnO_4 tetrahedra (in contrast, in the case of wurtzite, the ZnO_4

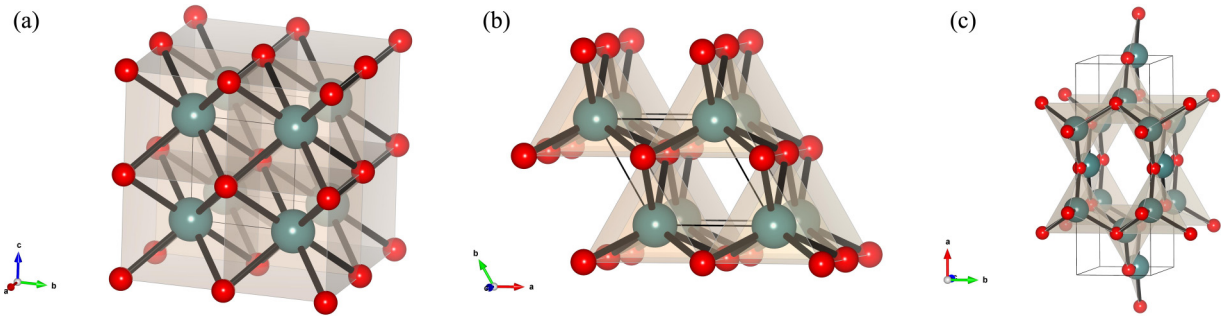

FIG. 4. (Color online) Visualization of structure types found at extreme high pressures: (a) CsCl type; (b) α-WC type; (c) ZnO-IV type.

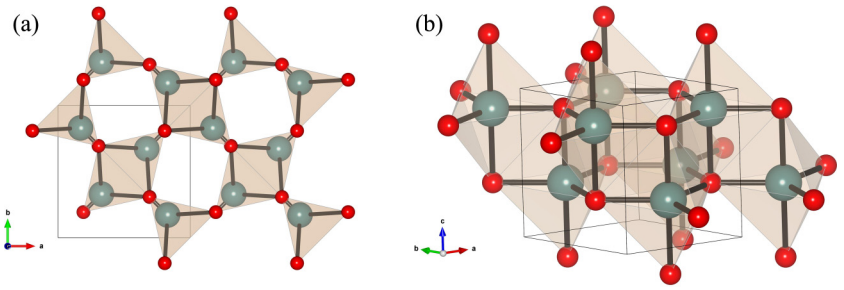

FIG. 5. (Color online) Visualization of the structure types found as minima at effective negative pressures: (a) β-BeO type; (b) 5-5 type.

tetrahedra are only connected via corners). A structure with these characteristics has recently been proposed by several theoretical groups as a possible phase in ZnO [95,96]. However, no assignment to a known structure type had been given—the structure was just denoted the *bct* structure based on its crystal lattice; using the CMPZ algorithm [79], we have found that this unknown phase corresponds to the β-BeO-type modification we have obtained from the global optimization (additional confirmation has been obtained from prescribed path calculations [87]). Recently, a cubane-type (CBE-ZnO) structure has been proposed [51]; however, we suggest that this is in reality a variation of the β-BeO-type modification, too.

From the $H(p)$ curves (see Fig. 6 and the Supplemental Material [77]), we see that on the HF level the transition from the wurtzite- to the β-BeO-type modification should occur at about -4 GPa and for the B3LYP functional at about -7 GPa. When using the LDA functional, this transition should take place beyond -10 GPa, and, even prior to this transition, the 5-5 modification might be observed as a (meta) stable phase. This structure type can be described as a mutual fivefold coordination of Zn cations by O anions in a hexagonal lattice ($P6_3/mmc$, no. 194) with *ABAB* stacking, where Zn atoms form trigonal bipyramids around O atoms and conversely, O atoms form trigonal bipyramids around Zn atoms [see Fig. 5(b)] [40,53]. The 5-5 structure type has been found on the energy landscapes of many AB compounds [40,41,91,93] in previous theoretical investigations of ZnO [18,86,87] and in experimental studies of very thin ZnO films

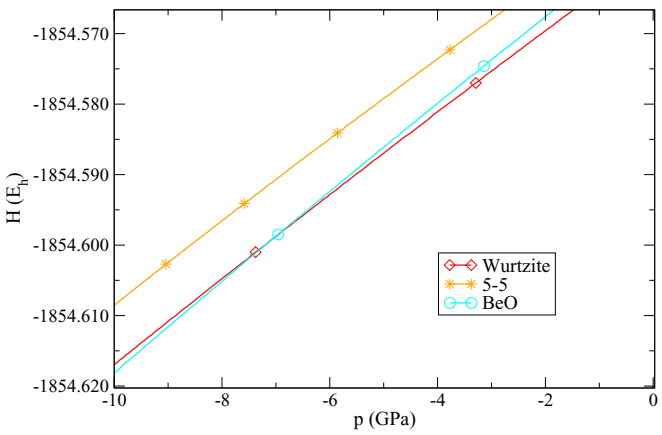

FIG. 6. (Color online) $H(p)$ curve for the relevant modifications of ZnO participating in the negative pressure region calculated using Hybrid (B3LYP) functional. Enthalpies per formula unit are given in hartrees (E_h).

(<15 atomic layers) [42,43]. Several groups have rediscovered this structure type in different contexts and have assigned various names to it, such as *h*-MgO.

Finally, the ZnO-IV type of structure has been found as another modification that may play a role in the low density region. The ZnO-IV modification [see Fig. 4(c)] resembles a zeolitic type of structure and exhibits space group *Imm*2 (no. 44). We note that this type of structure was stable regardless of the theoretical method employed. However, the phase transition is expected to occur only at very high negative pressures (after the β-BeO-type modification); therefore, its synthesis would most likely have to involve the use of templates similar to the case of zeolites.

B. Discussion

Our crystal structure prediction performed on zinc oxide over a wide range of pressures has produced a number of promising (meta)stable structure candidates that should be accessible experimentally in some pressure or temperature ranges, in addition to the experimentally known wurtzite, sphalerite, and rock salt modifications of bulk ZnO. Most notable among these are the β-BeO-, the GeP-, the 5-5-, the α-GeTe-, the α-WC-, and the CsCl-type modification. Additionally, we observe some polymorphs of ZnO of as yet unknown structure types, marked as ZnO-I to IV, as well as different stacking variants of wurtzite and sphalerite [97].

For large effective negative pressures that might occur in a low temperature atom beam-deposition synthesis (LT-ABD) [98,99], we would expect the β-BeO modification to be stable and appear as the outcome of the synthesis for some range of deposition parameters. Even at standard pressure, it might be possible to reach this modification, although at higher temperatures. We note that in the beryllium oxide system, two known modifications occur: α-BeO, which adopts the hexagonal wurtzite structure form, and β-BeO, a high temperature form that shows tetragonal symmetry [100]. By analogy, one might expect a similar relation to hold in the ZnO system, which would mean that at elevated temperatures one might be able to synthesize the β-BeO-type modification as a metastable phase in the ZnO system.

In contrast, the distorted α-GeTe-type modification belongs to the group of possible high pressure structures, where it would be in competition with the thermodynamically stable rock salt modification. Reaching this metastable structure appears to be rather difficult if one approaches the high pressure region by starting from the wurtzite modification since along this route the germanium phosphide modification is most likely to be encountered. However, recent investigations

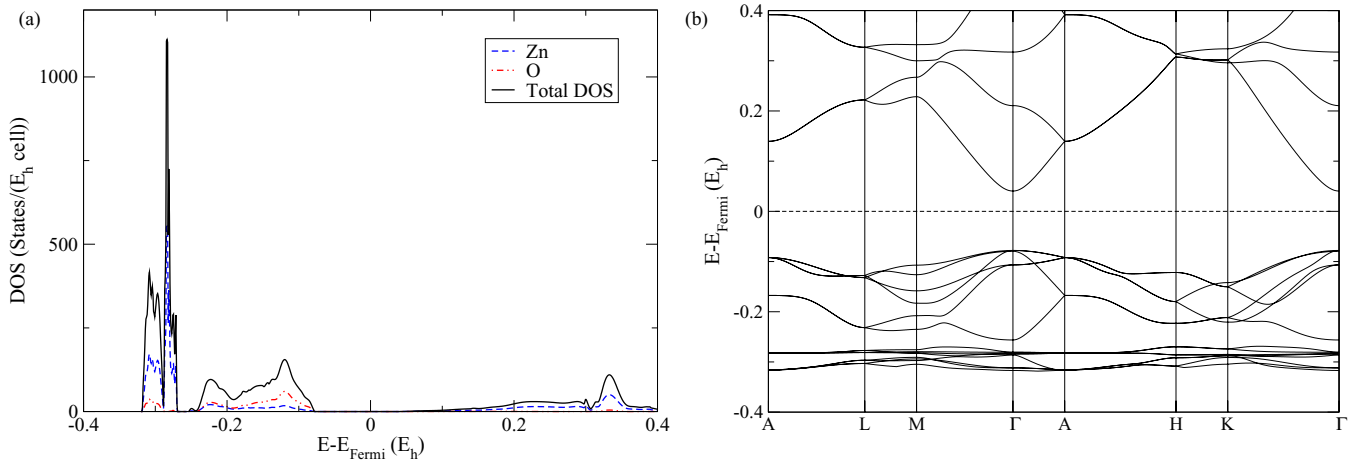

FIG. 7. (Color online) (a) Density of states (DOS) of the wurtzite modification. (b) Band structure of the wurtzite type at equilibrium volume showing a wide band gap. Calculation performed using hybrid B3LYP functional. Note that the labels of the special points of the Brillouin zones correspond to those of a hexagonal lattice.

of the transition route between the sphalerite modification and the rock salt modification on the zinc oxide energy landscape, using the prescribed path algorithm, show that the α-GeTe-type modification is found as one of the local minima along this transition path. We would therefore conclude that in order to observe the α-GeTe structure in the experiment, one should start from the sphalerite structure when applying pressure, while when starting from the wurtzite type of structure, one would most likely observe the GeP modification as an intermediate phase [87].

At extremely high pressures (>150 GPa), we observe a CsCl type of structure. Here, we suggest the α-WC modification as a possible intermediate phase along the NaCl $\rightarrow$ CsCl transition route at these extreme conditions.

Detailed investigations of the wurtzite-to-rock-salt transition route show that, besides the GeP-type modification, the 5-5-type modification is a noticeable minimum and metastable structure, which should be quite stable at low temperatures [87]. Similarly, the wurtzite-to-β-BeO transition path shows the 5-5 structure as an important minimum along this route. From the experiment, there is the evidence of very thin films of 5-5-type zinc oxide [42] and some tentative results from solution chemistry [43], which support the existence of the 5-5-type modification as a metastable bulk phase. Therefore, several routes appear to be open to the synthesis of bulk 5-5-type zinc oxide: growth of thick ZnO films at very low temperatures using the very thin 5-5-type films that can already be achieved as seeds; finding a refinement of the solution chemistry route; application of low temperatures and high pressures along the wurtzite-rock salt transition in the right combination of parameters; and finally, employing a synthesis like the LT-ABD method [98,99] to achieve the effective negative pressures required to make the 5-5-type modification thermodynamically stable compared to the wurtzite type.

During our research, we have encountered several rather interesting modifications, labeled as ZnO-I, -II, -III, and -IV, which one could not assign to a known structure prototype. However, we could describe the unknown ZnO-I and ZnO-II

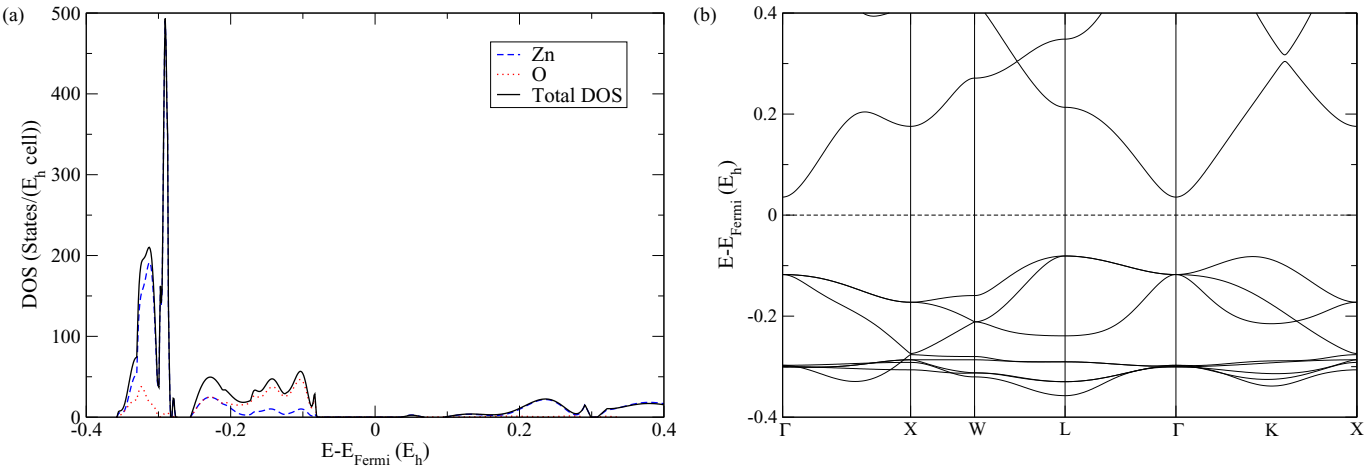

FIG. 8. (Color online) (a) Density of states (DOS) of the NaCl modification. (b) Band structure of the NaCl type at equilibrium volume showing a small direct band gap at the Γ-point and an indirect band gap (Γ-K or Γ-L). Calculation performed using hybrid B3LYP functional. Note that the labels of the special points of the Brillouin zones correspond to the ones of a face-centered cubic lattice.

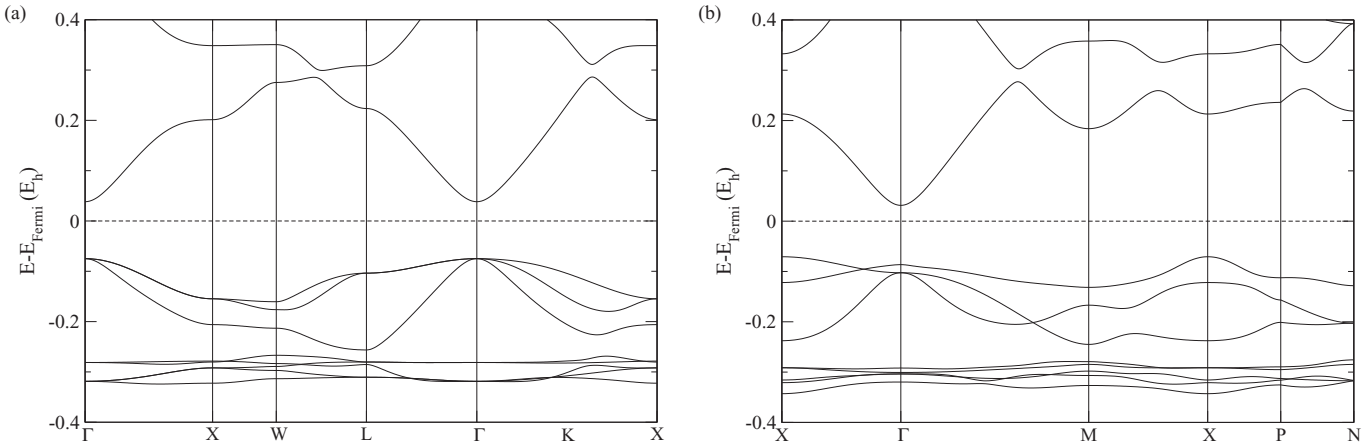

FIG. 9. Band structure calculation using the hybrid B3LYP functional for (a) sphalerite type and (b) GeP type. Note that in the GeP modification an indirect band gap (Γ-X) is observed, while in the sphalerite structure only the direct band gap at the Γ-point is present.

modifications as structures resulting from the distortions of the ideal rock salt structure. The ZnO-III modification can be considered as an alternative fivefold coordinated structure at elevated pressures, while the ZnO-IV modification, with its porous structure [see Fig. 4(c)], could be related to zeolite-type structures [22].

IV. ELECTRONIC PROPERTIES

A. Results

We have performed band structure and density of states (DOS) calculations for the various polymorphs of zinc oxide in order to gain additional insight into the electronic properties of the possible modifications of zinc oxide, which might suggest possible applications. The calculations were performed within the HF, DFT (LDA), and Hybrid (B3LYP) approximations. Our calculations were in good agreement with previous experimental [1,14,23,24,30,38,101–103] and theoretical findings [19,20,45–49,104] for those modifications where such calculations were available.

In the figures and tables presented in this section, we show the results for the most relevant modifications (wurtzite, sphalerite, NaCl, GeP, 5-5, and β-BeO) at their equilibrium volumes. Note that the labels of the special points of the brillouin zones of the wurtzite and the 5-5 type correspond to those of a hexagonal lattice. In the case of the sphalerite and NaCl structure, the special points correspond to the ones of a face-centered cubic lattice. For the GeP structure type, a simple tetragonal lattice was used, while in the case of the β-BeO structure the settings for a base-centered tetragonal lattice were applied, respectively.

In Figs. 7(a) and 7(b), we show DOS and band structure calculations of the ZnO wurtzite-type modification. We can confirm the previous experimental and theoretical investigations, where the direct band gap is observed at the Γ-point and where O 2p electrons mostly influence the valence band, while the next band is dominated by Zn 3d electrons. In Figs. 8(a) and 8(b), we show DOS and band structure calculations of the rock salt-type modification. We observe a somewhat larger direct band gap at the Γ-point and an indirect band gap at the L-point of the NaCl structure, and there are only slight changes in calculated DOS compared to the one of the wurtzite modification, which is in agreement with previous research [19,20,45–49,104].

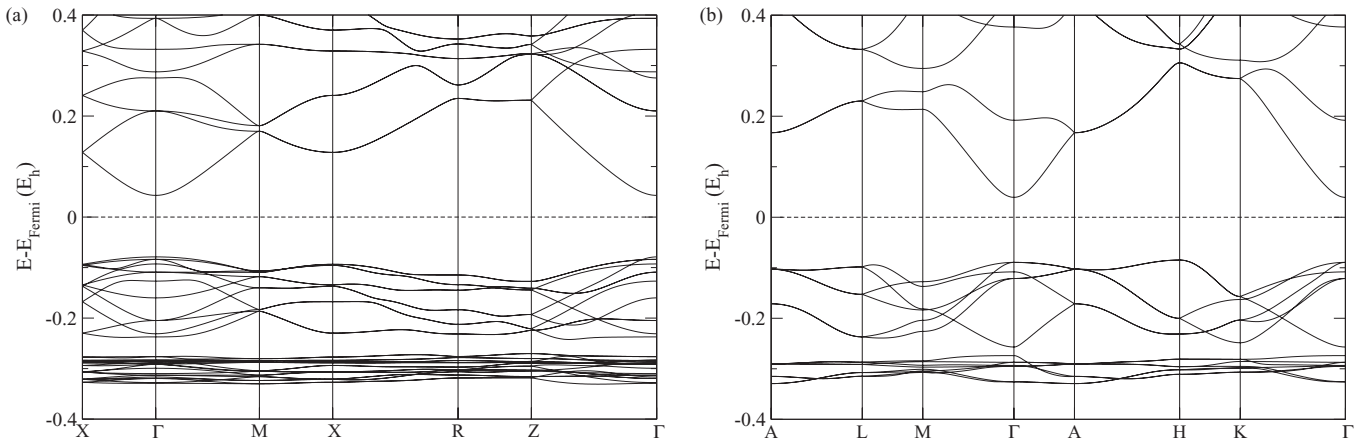

FIG. 10. Band structure calculation using the hybrid B3LYP functional for (a) β-BeO type and (b) 5-5 type. Note that in the 5-5 type modification, we observe an indirect band gap (Γ-H), while in the β-BeO type structure only the direct band gap at the Γ-point is present.

Furthermore, we show the band structure calculations for the most relevant alternative ZnO modifications within the B3LYP approximation: the sphalerite type [Fig. 9(a)], the GeP type [Fig. 9(b)], the β-BeO type [Fig. 10(a)], and the 5-5 type [Fig. 10(b)]. An important issue is that by using these additional ZnO modifications in technological applications, one could tune the band gap, decreasing it by integrating the wurtzite modification with, e.g., the sphalerite and the GeP type of structure (Fig. 9), or increasing the gap by adding elements of the β-BeO and the 5-5 type of structure. In addition, we observe that a small indirect gap appears in the GeP and 5-5 type of structure, while in the sphalerite- and β-BeO-type modification, only the direct band gap at the Γ-point is observed.

B. Discussion

Zinc oxide has a relatively large direct band gap of $\sim$3.3 eV, which has many advantages such as higher breakdown voltages, the ability to maintain large electric fields, applications in a high temperature and high power operation, etc. In the literature, the band gap of zinc oxide has been tuned to values between three and four eV by doping with magnesium oxide or cadmium oxide [1,105–107]. In our research we offer a new possibility of tuning the band gap in pure ZnO by employing different zinc oxide modifications.

The summary of the calculated direct band gaps of the most relevant ZnO modifications by using HF, DFT (LDA), and hybrid (B3LYP) functionals is shown in Table III. We observe that the band gaps of the nonequilibrium structures, both in the high pressure and in the negative pressure regions, are larger than the ones of the equilibrium modifications. We also note that no matter the calculation method applied or transition route chosen (e.g., the high pressure route wurtzite $\rightarrow$ 5-5 $\rightarrow$ GeP $\rightarrow$ NaCl or the effective negative-pressure route wurtzite $\rightarrow$ 5-5 $\rightarrow$ β-BeO [Ref. [87]) the size of the band gap increases, although the 5-5 modification slightly deviates from this trend (see Table III).

In addition, we observe an influence of the structure type on the indirect band gap, which is summarized in Table IV. Such an indirect band gap has been observed in the NaCl, the GeP, and the 5-5 modifications (see Figs. 8–10). We note that the size of the indirect gap has similar characteristic as the direct band gap, i.e., it is strongly underestimated by LDA and largely overestimated by the HF approximation. The surprising part was that calculations performed using HF gave us a smaller energy difference between the computed band gaps ($E_{\mathrm{dif}} = E_{\mathrm{dir}} - E_{\mathrm{ind}}$) than the one compute with the LDA functional.

TABLE III. Computed size of the direct band gap of the most relevant ZnO modifications. Calculations were performed with Hartree-Fock (HF), DFT (LDA), and hybrid (B3LYP) functionals. Note that the band gap is expressed in eV units.

	Method (eV)		
Structure type	LDA	B3LYP	HF
Wurtzite	1.24	3.21	11.78
Sphalerite	1.12	3.08	11.57
NaCl	2.88	4.17	12.86
GeP	1.68	3.20	12.03
5-5	1.70	3.49	12.23
β-BeO	1.31	3.31	11.83

TABLE IV. Computed size of the indirect band gap in ZnO system: the NaCl, the GeP, and the 5-5 modifications. Calculations were performed using Hartree-Fock (HF), DFT (LDA), and hybrid (B3LYP) functionals. Note that the band gap is expressed in eV units.

	Method (eV)		
Structure type	LDA	B3LYP	HF
NaCl	1.44	3.14	12.14
GeP	1.08	2.78	11.46
5-5	1.56	3.39	12.16

V. CONCLUSION

To gain new insights in the ZnO system, we have performed crystal structure prediction using simulated annealing with an empirical potential and on *ab initio* level, both at standard and elevated pressure. We have found the experimentally observed structure types (wurtzite, sphalerite, and rock salt) in agreement with previous research. In addition, many new interesting modifications were observed in different regions of the energy landscape. For example, we have found the nickel-arsenide (NiAs) type ($B8_1$) as a metastable modification at standard conditions, and at slightly negative pressures we observe the β-BeO type. Both at slightly elevated and slight negative pressures, we also find the so-called 5-5 type, which should be accessible as a metastable phase. Along the B4 $\rightarrow$ B1 transition path at high pressures, one might also encounter the GeP phase, and several metastable modifications, in particular the α-WC type, are suggested as possible high pressure phases in the zinc oxide system before one reaches the CsCl-type phase at very high pressures.

In the second part of this study, we have investigated the electronic properties of the most relevant stable structures identified during the global explorations. Our calculations were in good agreement with previous theoretical findings when available; here, calculations with the hybrid functional (B3LYP) show the closest agreement of the band gap with the experimental observations. Additionally to the band structures of the experimentally know modifications, we discuss the electronic properties of the possible alternative ZnO modifications within the B3LYP approximation. In particular, several of the new proposed modifications show an indirect band gap. These new findings offer new possibilities of tuning the band gap in pure ZnO via combinations of different structural arrangements.

ACKNOWLEDGMENTS

The authors would like to thank K. Doll, I. Pentin, B. Matovic, U. Wedig, and J. Nuss for valuable discussions.

TABLE V. Results of the structural crystallographic analysis of the global optimizations at standard pressure in ZnO for a different number of formula units (Z) and radius scale factor (r_s). Only predominantly found structures are listed.

r_{Zn}	r_O	$Z=1$	$Z=2$	$Z=3$	$Z=4$	$Z=5$
		Dist. sph (B3)	Wur. (B4)	Sph. (B3)	β-BeO	Dist. β-BeO
0.7	1.2	*CmCm*	$P6_3mc$	F-43m	$P4_2/mnm$	*Amm*2
		(no. 8)	(no. 186)	(no. 216)	(no. 136)	(no. 38)
		Dist. sph (B3)	Wur. (B4)	Sph. (B3)	β-BeO	Dist. β-BeO
0.7	1.3	*CmCm*	$P6_3mc$	F-43m	$P4_2/mnm$	*Amm*2
		(no. 8)	(no. 186)	(no. 216)	(no. 136)	(no. 38)
		Dist. sph (B3)	NaCl (B1)	GeP	NaCl (B1)	Amorphous
0.8	1.2	*CmCm*	*Fm*-3*m*	*I*4*mm*	*Fm*-3*m*	$P1$
		(no. 8)	(no. 225)	(no. 107)	(no. 225)	(no. 1)
		Dist. sph (B3)	5-5	Sph. (B3)	β-BeO	Dist. β-BeO
0.8	1.3	*CmCm*	$P6_3/mmc$	F-43m	$P4_2/mnm$	*Amm*2
		(no. 8)	(no. 194)	(no. 216)	(no. 136)	(no. 38)
		Dist. sph (B3)	Wur. (B4)	Sph. (B3)	β-BeO	Dist. β-BeO
0.8	1.4	*CmCm*	$P6_3mc$	F-43m	$P4_2/mnm$	*Amm*2
		(no. 8)	(no. 186)	(no. 216)	(no. 136)	(no. 38)

APPENDIX

1. Statistical analysis of the optimization process, calculated total energies, and bulk moduli

Global searches were performed at seven different pressure (p) settings (from -10 GPa to 1000 GPa) with five different settings for radius scale factor (r_s) and five different sizes of unit cell (Z), where for each set of p, r_s, and Z, 400 SA runs were employed. A summary of the results of the global optimization at standard pressure in the zinc oxide system as function of the radius scale factor r_s Ref. [40] that was varied for the Zn^{2+} and the O^{2-} ion, and of the number of formula units in the simulation cell Z, is given in Table V. In each case, the most frequently observed minimum is listed. For one formula unit ($Z=1$), besides the sphalerite and the NaCl type of structures, only a strongly distorted sphalerite intermediate in space group *Cm* (no. 8) appeared. For $Z=2$, wurtzite was the most dominant structure type, showing space group $P6_3mc$ (no. 186), although there were radius settings of the Zn and O ions, where the NaCl (*Fm*-3*m*, no. 225) and the 5-5 ($P6_3/mmc$, no. 194) structure type were reached more frequently than the wurtzite structure on the energy landscape of ZnO. Here, we note that this occurred even though the energy of the wurtzite structure was still the lowest of all configurations found. With the calculations performed for three formula units, the sphalerite structure type (space group F-43m, no. 216) was the minimum reached most often. Again, there was a setting of the radius scale factors [r_s(Zn) = 0.8, r_s(O) = 1.2], which favored the GeP structure type (*I*4*mm*, no. 107).

For $Z=4$, in most of the calculations we have found the minima belonging to the β-BeO structure type, exhibiting

TABLE VI. Overview of the structural crystallographic analysis of the global optimization calculations performed at various elevated pressures in ZnO for a different number of formula units (Z) and radius scale factor (r_s). The pressure during the calculations was set to $p=1$ MPa, 10 MPa, 100 MPa, 1 GPa, 10 GPa, and 100 GPa. Note that only predominantly found structures are listed.

r_{Zn}	r_O	$Z=1$	$Z=2$	$Z=3$	$Z=4$	$Z=5$
		NaCl (B1)	5-5	NaCl (B1)	NaCl (B1)	Amorphous
0.7	1.2	*Fm*-3*m*	$P6_3/mmc$	*Fm*-3*m*	*Fm*-3*m*	$P1$
		(no. 225)	(no. 194)	(no. 225)	(no. 225)	(no. 1)
		NaCl (B1)	NaCl (B1)	Amorphous	NaCl (B1)	Dist. β-BeO
0.7	1.3	*Fm*-3*m*	*Fm*-3*m*	$P1$	*Fm*-3*m*	*Amm*2
		(no. 225)	(no. 225)	(no. 1)	(no. 225)	(no. 38)
		NaCl (B1)	NaCl (B1)	GeP	NaCl (B1)	Amorphous
0.8	1.2	*Fm*-3*m*	*Fm*-3*m*	*I*4*mm*	*Fm*-3*m*	$P1$
		(no. 225)	(no. 225)	(no. 107)	(no. 225)	(no. 1)
0.8	1.3	Dist. sph/NaCl (B3/B1)	ZnO-I	GeP	NaCl (B1)	Amorphous
		CmCm	$P2_1/m$	*I*4*mm*	*Fm*-3*m*	$P1$
		(no. 8)	(no. 11)	(no. 107)	(no. 225)	(no. 1)
		Dist. ZnS/NaCl	NaCl (B1)	NaCl (B1)	NaCl (B1)	Amorphous
0.8	1.4	*CmCm*	*Fm*-3*m*	*Fm*-3*m*	*Fm*-3*m*	$P1$
		(no. 8)	(no. 225)	(no. 225)	(no. 225)	(no. 1)

TABLE VII. Calculated total energies of the most relevant ZnO modifications. Local optimizations were performed within Hartree-Fock (HF), DFT (LDA), and hybrid (B3LYP) approximation. Note that the energies are calculated for equilibrium volumes and expressed in Hartrees (E_h) per one formula unit ($Z = 1$) with precision of 10^{-4} E_h.

Structure	Energy (E_h)		
type	LDA	B3LYP	HF
Wurtzite	−1851.2629	−1854.5584	−1852.7170
Sphalerite	−1851.2632	−1854.5575	−1852.7143
NaCl	−1851.2554	−1854.5441	−1852.7069
GeP	−1851.2561	−1854.5458	−1852.7055
5-5	−1851.2563	−1854.5503	−1852.7114
NiAs	−1851.2534	−1854.5389	−1852.6963
BeO	−1851.2597	−1854.5553	−1852.7145
CsCl	−1851.2214	−1854.4995	−1852.6488

space group ($P4_2/mnm$, no. 136), although there were again radius scale settings where, e.g., the NaCl type was reached most often. When we performed calculations for five formula units, we observed only distortions of all the structure types mentioned, the most common one in the space groups $Amm2$ (no. 38) or $P1$ (no. 1). This is not a surprise, since, with the exception of the sphalerite and rock salt types, none of the other structure types can be represented by a periodically repeated unit cell containing exactly five formula units. Our experience with other chemical systems has shown that using five or seven formula units tends to produce structures with the same local coordination polyhedra as the optimal structures but rather unusual networks of these polyhedra.

An analogous summary of the high pressure calculations is given in Table VI. We observe that the most frequent minimum on the high pressure landscapes of ZnO corresponds to the NaCl structure type. Again, for different values of Z and r_s [40], we observe different distortions of the NaCl structure type, e.g., in the space group Cm (no. 8) or $P2_1/m$ (no. 11), or structures that are related to perfect NaCl, e.g., the 5-5 or the GeP structure type. If we increase the number of formula units to $Z = 5$, then in most cases we observe structures without any additional symmetry elements ($P1$, no. 1). The structure candidates that were obtained with the radius scale factors of $r_s(\mathrm{Zn}) = 0.8$ and $r_s(\mathrm{O}) = 1.4$ in the global and local optimizations were chosen for calculations that explored the barrier landscape in more detail by using the so-called threshold [110] and the prescribed path algorithm [87].

Calculated total energies of the most relevant ZnO modifications after local optimizations with the HF, the DFT (LDA), and the hybrid (B3LYP) approximation, respectively, are shown in Table VII. Additionally, calculated total energies of the most relevant ZnO modifications and their corresponding volumes, energy differences in temperature units, and bulk moduli—all computed with the hybrid B3LYP functional—can be found in Table VIII. Our calculations show good agreement with previously calculated and experimentally observed bulk moduli.

TABLE VIII. Calculated total energies of the most relevant ZnO modifications, their corresponding temperatures, and bulk moduli. Calculation performed using hybrid B3LYP functional. Note that the energies are calculated for equilibrium volumes and expressed in Hartrees (E_h) per one formula unit ($Z = 1$).

Structure	Energy	Volume	Temperature*	Bulk modulus(GPa)		
type	(E_h)	(A^3)	(K)	B3LYP	Exp.	Theo.
Wurtzite	−1854.5584	24.5945	0	146	139.6[a]	131.5[c]
					183[b]	154.4[d]
Sphalerite	−1854.5575	24.6426	+285	132	–	131.6[c]
						156.8[d]
NaCl	−1854.5441	19.9059	+4500	223	228[b]	167.8[c]
					218[e]	203.3[d]
GeP	−1854.5458	21.5935	+4000	151	–	–
5-5	−1854.5503	23.6196	+2500	127	–	–
NiAs	−1854.5389	20.6036	+6150	169	–	–
BeO	−1854.5553	25.2959	+980	121	–	–
CsCl	−1854.4995	19.3663	+18600	177	–	162.4[c]
						194,3[f]

*The temperature is expressed as the energy difference to the wurtzite modification, converted from Haretree (E_h) to Kelvin (K).
[a]Ref. [33]
[b]Ref. [108]
[c]Ref. [109]
[d]Ref. [73]
[e]Ref. [35]
[f]Ref. [19]

[1] Ü. Özgür, Ya. I. Alivov, C. Liu, A. Teke, M. A. Reshchikov, S. Doğan, V. Avrutin, S.-J. Cho, and H. Morkoç, J. Appl. Phys. **98**, 041301 (2005).

[2] A. Hernandez-Battez, R. González, J. L. Viesca, J. E. Fernández, J. M. Díaz Fernández, A. Machado, R. Chou, and J. Riba, Wear **265**, 422 (2008).

[3] H. Sawada, R. Wang, and A. W. Sleight, J. Sol. Stat. Chem. **122**, 148 (1996).

[4] T.-B. Hur, G. S. Jeen, Y.-H. Hwang, and H.-K. Kim, J. Appl. Phys. **94**, 5787 (2003).

[5] Z. Zhou, K. Kato, T. Komaki, M. Yoshino, H. Yukawa, M. Morinaga, and K. Morita, J. Eur. Ceram. Soc. **24**, 139 (2004).

[6] T. Suski and W. Paul, *High Pressure in Semiconductor Physics I, Semiconductors and Semimetals*, Vol. 54, (Academic Press, San Diego, 1998).

[7] C. Klingshirn, Chem. Phys. Chem. **8**, 782 (2007).

[8] D. Lukovic Golic, G. Brankovic, M. Pocuca Nesic, K. Vojisavljevic, A. Recnik, N. Daneu, S. Bernik, M. Scepanovic, D. Poleti, and Z. Brankovic, Nanotechnology **22**, 395603 (2011).

[9] Y. W. Heo, D. P. Norton, L. C. Tien, Y. Kwon, B. S. Kang, F. Ren, S. J. Pearton, and J. R. LaRoche, Mater. Sci. Eng. R **47**, 1 (2004).

[10] P. Lipowsky, Z. Burghard, L. P. H. Jeurgens, J. Bill, and F. Aldinger, Nanotechnology **18**, 345707 (2007).

[11] I. Kuryliszyn-Kudelska, B. Hadzic, D. Sibera, M. Romcevic, N. Romcevic, U. Narkiewicz, W. Lojkowski, M. Arciszewska, and W. Dobrowolski, J. Alloy. Compd. **561**, 247 (2013).

[12] M. Behrens, G. Lolli, N. Muratova, I. Kasatkin, M. Havecker, R. Naumann d'Alnoncourt, O. Storcheva, K. Kohler, M. Muhlerd, and R. Schlogla, Phys. Chem. Chem. Phys. **15**, 1374 (2013).

[13] M. Liu, G.-B. Ma, X. Xiong, Z.-W. Wang, R.-W. Peng, J.-G. Zheng, D.-J. Shu, Z. Zhang, and M. Wang, Phys. Rev. B **87**, 085306 (2013).

[14] M. Šćepanović, M. Grujić-Brojčin, K. Vojisavljević, and T. Srećković, J. Appl. Phys. **109**, 034313 (2011).

[15] J. Y. Lao, J. G. Wen, and Z. F. Ren, Nano Lett. **2**, 1287 (2002).

[16] C. R. A. Catlow, S. A. French, A. A. Sokol, A. A. Al- Sunaidi, and S. M. Woodley, J. Comput. Chem. **29**, 2234 (2008).

[17] P. Erhart, N. Juslin, O. Goy, K. Nordlund, R. Muller, and K. Albe, J. Phys.: Condens. Matter **18**, 6585 (2006).

[18] A. J. Kulkarni, M. Zhou, K. Sarasamak, and S. Limpijumnong, Phys. Rev. Lett. **97**, 105502 (2006).

[19] J. E. Jaffe, J. A. Snyder, Z. Lin, and A. C. Hess, Phys. Rev. B **62**, 1660 (2000).

[20] Z. Zeng, C. S. Garoufalis, S. Baskoutas, and G. Bester, Phys. Rev. B **87**, 125302 (2013).

[21] A. Kawska, P. Duchstein, O. Hochrein, and D. Zahn, Nano Lett. **8**, 2336 (2008).

[22] M. A. Zwijnenburg and S. T. Bromley, J. Mater. Chem. **21**, 15255 (2011).

[23] W. Hu, Z. Li, and J. Yang, J. Chem. Phys. **138**, 124706 (2013).

[24] A. Kronenberger, A. Polity, D. M. Hofmann, B. K. Meyer, A. Schleife, and F. Bechstedt, Phys. Rev. B **86**, 115334 (2012).

[25] S. E. Boulfelfel and S. Leoni, Phys Rev. B **78**, 125204 (2008).

[26] B. G. Kim, Phys. Rev. Lett. **108**, 259601 (2012).

[27] W. D. Nesse, *Introduction to Mineralogy* (Oxford University Press, New York, 2000).

[28] M. Allaby, *Dictionary of Earth Sciences* (Oxford University Press, New York, 2008).

[29] J. W. Anthony, R. A. Bideaux, K. W. Bladh, and M. C. Nichols, *Handbook of Mineralogy* (Mineralogical Society of America, Chantilly, Virginia, USA, 2013).

[30] B. Predel and O. Madelung, *O-Zn (Oxygen-Zinc)* (Springer Materials—The Landolt-Bornstein Database, Berlin, Heidelberg, Germany, 2013).

[31] H. Sowa and H. Ahsbahs, J. Appl. Cryst. **39**, 169 (2006).

[32] C. H. Bates, W. B. White, and R. Roy, Science **137**, 993 (1962).

[33] H. Liu, Y. Ding, M. Somayazulu, J. Qian, J. Shu, D. Häusermann, and H.-K. Mao, Phys. Rev. B **71**, 212103 (2005).

[34] H. Karzel, U. Potzel, W. Potzel, J. Moser, C. Schaefer, M. Steiner, M. Peter, A. Kratzer, and G. M. Kalvius, Mater. Sci. Forum **79**, 419 (1991).

[35] F. Decremps, F. Datchi, A. M. Saitta, A. Polian, S. Pascarelli, A. Di Cicco, J. P. Itie, and F. Baudelet, Phys. Rev. B **68**, 104101 (2003).

[36] W. Bragg and J. A. Darbyshire, Trans. Farad. Soc. **28**, 522 (1932).

[37] T. Kogure and Y. Bando, J. Elec. Microscopy **47**, 135 (1998).

[38] S.-K. Kim, S.-Y. Jeong, and C. R. Cho, Appl. Phys. Lett. **82**, 562 (2003).

[39] A. B. M. A. Ashrafi, A. Ueta, A. Avramescu, H. Kumano, I. Suemune, Y. Ok, and T. Seong, Appl. Phys. Lett. **76**, 550 (2000).

[40] J. C. Schön and M. Jansen, Comp. Mater. Sci. **4**, 43 (1995).

[41] D. Zagorac, J. C. Schön, and M. Jansen, Process. Appl. Ceram. **7**, 37 (2013).

[42] C. L. Pueyo, S. Siroky, S. Landsmann, M. W. E. van den Berg, M. R. Wagner, J. S. Reparaz, A. Hoffmann, and S. Polarz, Chem. Mater. **22**, 4263 (2010).

[43] C. Tusche, H. L. Meyerheim, and J. Kirschner, Phys. Rev. Lett. **99**, 026102 (2007).

[44] F. Claeyssens, C. L. Freeman, N. L. Allan, Y. Sun, M. N. R. Ashfold, and J. H. J. Harding, Mater. Chem. **15**, 139 (2005).

[45] J. Sun, H.-T. Wang, J. He, and Y. Tian, Phys. Rev. B **71**, 125132 (2005).

[46] B. Amrani, I. Chiboub, S. Hiadsi, T. Benmessabih, and N. Hamdadou, Solid State Commun. **137**, 395 (2006).

[47] J. Wrobel and J. Piechota, Solid State Commun. **146**, 324 (2008).

[48] Z. Li, Y. Xu, G. Gao, T. Cui, and Y. Ma, Phys. Rev. B **79**, 193201 (2009).

[49] S. Cui, W. Feng, H. Hu, Z. Feng, and Y. Wang, J. Alloy. Compd. **476**, 306 (2009).

[50] M. Kalay, H. H. Kart, S. Ö. Kart, and T. Cagın, J. Alloy. Compd. **484**, 431 (2009).

[51] S. Zhang, Y. Zhang, S. Huang, P. Wang, and H. Tian, Chem. Phys. Lett. **557**, 102 (2013).

[52] Y. Mori, N. Niiya, K. Ukegawa, T. Mizuno, K. Takarabe, and A. L. Ruoff, Phys. Status Solidi B **241**, 3198 (2004).

[53] D. Zagorac, J. C. Schön, I. Pentin, and M. Jansen, Process. Appl. Ceram. **5**, 73 (2011).

[54] D. Zagorac, J. C. Schön, and M. Jansen, Acta Phys. Pol. A **120**, 215 (2011).

[55] J. C. Schön and M. Jansen, Angew. Chem., Int. Ed Eng. **35**, 1268 (1996).

[56] J. C. Schön, K. Doll, and M. Jansen, Phys. Status Solidi (b) **247**, 23 (2010).

[57] S. Kirkpatrick, C. D. Gelatt, and M. P. Vecchi, Science **220**, 671 (1983).

[58] M. Jansen, K. Doll, and J. C. Schön, Acta Crystallogr. A **66**, 518 (2010).

[59] S. W. de Leeuw, J. W. Perram, and E. R. Smith, Proc. Roy. Soc. London A **373**, 27 (1980).

[60] S. Neelamraju, J. C. Schön, K. Doll, and M. Jansen, Phys. Chem. Chem. Phys. **14**, 1223 (2012).

[61] R. Dovesi, R. Orlando, B. Civalleri, C. Roetti, V. R. Saunders, and C. M. Zicovich-Wilson, Z. Kristallogr. **220**, 571 (2005).

[62] R. Dovesi, V. R. Saunders, C. Roetti, R. Orlando, C. M. Zicovich-Wilson, F. Pascale, B. Civalleri, K. Doll, N. M. Harrison, I. J. Bush, P. D'Arco, and M. Llunell, *CRYSTAL09 User's Manual* (University of Torino, Torino, Italy, 2009).

[63] B. Civalleri, P. D'Arco, R. Orlando,V. R. Saunders, and R. Dovesi, Chem. Phys. Lett. **348**, 131 (2001).

[64] K. Doll, V. R. Saunders, and N. M. Harrison, Int. J. Quantum Chem. **82**, 1 (2001).

[65] K. Doll, Comput. Phys. Commun. **137**, 74 (2001).

[66] K. Doll, R. Dovesi, and R. Orlando, Theor. Chem. Acc. **112**, 394 (2004).

[67] J. Slater and H. C. Verma, Phys. Rev. **34**, 1293 (1929).

[68] J. C. Slater, *The Self-Consistent Field for Molecular and Solids, Quantum Theory of Molecular and Solids*, Vol. 4 (McGraw-Hill, New York, 1974).

[69] J. P. Perdew and A. Zunger, Phys. Rev. B **23**, 5048 (1981).

[70] A. Becke, J. Chem. Phys. **98**, 5648 (1993).

[71] J. C. Schön, Z. P. Cancarevic, and M. Jansen, J. Chem. Phys. **121**, 2289 (2004).

[72] K. Doll and M. Jansen, Angew. Chem. **123**, 4723 (2011).

[73] J. E. Jaffe and A. C. Hess, Phys. Rev. B **48**, 7903 (1993).

[74] T. Homann, U. Hotje, M. Binnewies, A. Borger, K. D. Becker, and T. Bredow, Solid State Sci. **8**, 44 (2006).

[75] M. D. Towler, N. L. Allan, N. M. Harrison, V. R. Saunders, W. C. Mackrodt, and E. Aprà, Phys. Rev. B **50**, 5041 (1994).

[76] A. M. Ferrari and C. Pisani, J. Phys. Chem. **110**, 7909 (2006).

[77] See Supplemental Material at http://link.aps.org/supplemental/10.1103/PhysRevB.89.075201 for the basis set information and additional $E(V)$ and $H(p)$ curves.

[78] A. Hannemann, R. Hundt, J. C. Schön, and M. Jansen, J. Appl. Crystallogr. **31**, 922 (1998).

[79] R. Hundt, J. C. Schön, and M. Jansen, J. Appl. Crystallogr. **39**, 6 (2006).

[80] R. Hundt, *KPLOT program-Version 9. 6.15* (University of Bonn, Germany, 2012).

[81] K. Momma and F. Izumi, J. Appl. Crystallogr. **41**, 653 (2008).

[82] M. P. Molepo and D. P. Joubert, Phys. Rev. B **84**, 094110 (2011).

[83] S. Limpijumnong and S. Jungthawan, Phys. Rev. B **70**, 054104 (2004).

[84] J. Frenzel, G. Seifert, and D. Zahn, Z. Anorg. Allg. Chem. **635**, 1773 (2009).

[85] F.-Y. Zhang, Physica. B **406**, 3942 (2011).

[86] J. Cai and N. J. Chen, Phys. Rev. B **75**, 134109 (2007).

[87] D. Zagorac, J. C. Schön, and M. Jansen, J. Phys. Chem. C **116**, 16726 (2012).

[88] T. Nonaka, G. Ohbayashi, Y. Toriumi, Y. Mori, and H. Hashimoto, Thin Solid Films **370**, 258 (2000).

[89] P. Fons, A. V. Kolobov, M. Krbal, J. Tominaga, K. S. Andrikopoulos, S. N. Yannopoulos, G. A. Voyiatzis, and T. Uruga, Phys. Rev. B **82**, 155209 (2010).

[90] G.-S. Do, J. Kim, S.-H. Jhi, C.-H. Park, S. G. Louie, and M. L. Cohen, Phys. Rev. B **82**, 054121 (2010).

[91] D. Zagorac, K. Doll, J. C. Schön, and M. Jansen, Phys. Rev. B **84**, 045206 (2011).

[92] D. Zagorac, K. Doll, J. C. Schön, and M. Jansen, Chem. Eur. J. **18**, 10929 (2012).

[93] Ž. Cancarevic, J. C. Schön, and M. Jansen, Chem. Asian J. **3**, 561 (2008).

[94] D. V. Suetin, I. R. Shein, and A. L. Ivanovskii, J. Phys. Chem. Solids **70**, 64 (2009).

[95] B. J. Morgan, Phys. Rev. B **82**, 153408 (2010).

[96] J. Wang, P. Xiao, M. Zhou, Z. R. Wang, and F. J. Ke, J. Appl. Phys. **107**, 023512 (2010).

[97] D. Zagorac, J. C. Schön, J. Zagorac, and M. Jansen (unpublished).

[98] The low temperature atom beam-deposition method proceeds by depositing an atomically disperse mixture of the participating atom species on a cooled substrate (liquid nitrogen or liquid helium temperatures), thus generating an amorphous matrix. Upon slowly tempering at low temperatures, nuclei of various stable and metastable phases are formed, where the low density phases are preferred due to the effective negative pressure exerted by the amorphous low density matrix on the denser crystalline nuclei [99].

[99] D. Fischer and M. Jansen, J. Am. Chem. Soc. **124**, 3488 (2002).

[100] D. K. Smith, C. F. Cline, and S. B. Austerman, Acta Cryst. **18**, 393 (1965).

[101] A. Mang, K. Reimann, and S. Rubenacke, Solid State Commun. **94**, 251 (1995).

[102] D. Milivojevic, B. Babic-Stojic, and J. Kovac, App. Surf. Sci. **257**, 937 (2010).

[103] K. Siraj, K. Javaid, J. D. Pedarnig, M. A. Bodea, and S. Naseem, J. Alloys Compd. **563**, 280 (2013).

[104] S. H. Jang and S. F. Chichibu, J. Appl. Phys. **112**, 073503 (2012).

[105] A. Ohtomo, M. Kawasaki, T. Koida, K. Masubuchi, and H. Koinuma, Appl. Phys. Lett. **72**, 2466 (1998).

[106] A. Janotti and C. G. Van De Walle, Nat. Mater. **6**, 44 (2007).

[107] Y.-S. Choi, C.-C. Lee, and S. M. Cho, Thin Solid Films **289**, 153 (1996).

[108] H. Karzel, W. Potzel, M. Kofferlein, W. Schiessl, M. Steiner, U. Hiller, G. M. Kalvius, D. W. Mitchell, T. P. Das, P. Blaha, K. Schwarz, and M. P. Pasternak, Phys. Rev. B **53**, 11425 (1996).

[109] A. Schleife, F. Fuchs, J. Furthmüller, and F. Bechstedt, Phys. Rev. B **73**, 245212 (2006).

[110] J. C. Schön, H. Putz, and M. Jansen, J. Phys.: Condens. Matter **8**, 143 (1996).